Science in China Series G: Physics, Mechanics & Astronomy

www.scichina.com
phys.scichina.com
www.springerlink.com

Numerical study on transient flow in the deep naturally fractured reservoir with high pressure

LIU YueWu†, CHEN WeiLiang & LIU QingQuan

Division of Engineering Science, Institute of Mechanics, Chinese Academy of Sciences, Beijing 100190, China

According to the experimental results and the characteristics of the pressure-sensitive fractured formation, a transient flow model is developed for the deep naturally-fractured reservoirs with different outer boundary conditions. The finite element equations for the model are derived. After generating the unstructured grids in the solution regions, the finite element method is used to calculate the pressure type curves for the pressure-sensitive fractured reservoir with different outer boundaries, such as the infinite boundary, circle boundary and combined linear boundaries, and the characteristics of the type curves are comparatively analyzed. The effects on the pressure curves caused by pressure sensitivity module and the effective radius combined parameter are determined, and the method for calculating the pressure-sensitive reservoir parameters is introduced. By analyzing the real field case in the high temperature and pressure reservoir, the perfect results show that the transient flow model for the pressure-sensitive fractured reservoir in this paper is correct.

seepage, transient flow, mathematical model, numerical method, fractured reservoir, high pressure

With the improvement of the oilfield development technology and the growing demand for oil and gas resources, deeper and deeper high-pressure reservoirs are developed. Because of the high pressure and temperature in the deep oil and gas reservoirs, the formation will be changed with partial or whole irreversible deformation during the development of the reservoir. With formation deformation, as well as the variable properties of liquids and gases, the reservoir dynamic characteristics will obviously be affected. Without correct understanding the transient flow mechanics in such reservoir, the well productivity will not be given reasonable. In such reservoir, the well productivity will decrease sharply and can not be rebuilt by any method. The reservoir recovery will decrease sharply in result. According to refs. [1—4], the largest permeability loss is 90%, while the largest well producing rate loss is 50%.

In the current oil and gas reservoir developing process, the porous media deformation can be divided into three types: elastic deformation, plastic deformation and elastic-plastic deformation. Based on the analysis of the indoor experimental data, the high-pressure deep fractured reservoir mostly belongs to the second type, the plastic deformation reservoir. This type reservoir shows abnormal characteristics: The initially large opening crack due to the high fluid pressure in the crack reduces largely as the fluid pressure sharply drops. The reduced opening crack is difficult to be reopened even with a high level fluid pressure, resulting in that the reservoir porosity and permeability will continue to be decreased.

The pressure-sensitive fractured reservoir indicates that the reservoir properties change with the surrounding pressure in the porous media, and most of these kinds of changes are irreversible. The reservoir properties mentioned here are the properties of the skeleton, the porosity and the fluid. These properties can be described by the parameters of porous media and fluid, such as permeability, porosity, fluid compressibility, density, viscosity, and so on. According to the experimental data,

Received June 8, 2007; accepted December 14, 2008
doi: 10.1007/s11433-009-0121-2
†Corresponding author (email: lywu@imech.ac.cn)

Terzaghi[5] suggested that the variation of porosity can be ignored in the engineering calculation, but permeability changes must be considered.

Since 1925 Terzaghi[5] put forward the concept of effective stress in the study of soil consolidation theory, the seepage theory on deformable porous media has experienced a long development history. The development of effective stress principle has founded a basic theory for solving deformation problems in porous media. In 1955, Biot[6] extended Terzaghi's theory to the elastic consolidation theory in anisotropic porous media. Biot assumed that the fluid in a reservoir was compressible and viscous fluid. He distinguished solid framework stress from porous fluid pressure and differentiated solid frame deformation from fluid motion. In addition, he described the fluid flow relative to the solid framework in porous media by Darcy's law. He also proposed the stress-strain relationship for the problem with anisotropic visco-elasticity and the problem with relaxation phenomenon, which can be used to predict the stress-strain change history during the fluid flow in anisotropic porous media. In 1957, Geertsma[7], based on the previous research, created the poroelasticity theory and the corresponding relationships, and explicitly gave the definition of the rock volume compressibility and the pore compressibility as well as their relationship, which can be used quantitatively to determine the pore volume variation caused by the pore pressure change. In 1975, by considering the influence of the rock compaction effect on seepage flow and reservoir exploitation, Finol and Farouq Ali[8] developed a three-dimensional and two-phase seepage flow model, and solved it by using finite difference method. This seepage model was composed by oil and water seepage equation and an analytical equation group with the linear elastic deformation of the porous media. The model considered the effect that the variations of porosity and permeability caused by the rock compaction, which exerted on the final reservoir recovery. So this model was one typical model of the linear elastic deformation theory.

On the basis of the linear elastic seepage theory, the oil workers in the Soviet Union[9], developed some elastoplastic seepage models and plastic seepage models. They only modified the model by expressing the porosity and permeability variations in the form of index or power function of the fluid pressure drawdown. In 1972, Raghavan et al.[10] developed a pressure-sensitive homogeneous reservoir transient flow model, and gave a new formula of pseudo pressure. In this model, the change of permeability caused by the pressure variation was involved in the item of pseudo-pressure. So the model was changed from the nonlinear equations to the quasilinear equations, and the numerical solution for the pressure-sensitive problem was given. In 1977, Samaniego, Brigham and Miller[11] developed a transient flow model which considered the change of rock and fluid compressibility due to pressure variation. In 1983, Ostensen[12] mentioned the pressure sensitivity could cause the initial productivity to reduce up to 30% for typical tight sand gas reservoirs, and put forward that using the seepage model without the considering of pressure sensitivity to analyze the pressure transient behavior would cause an enormous deviation. In 1990, Pedrosa[13] developed a deformable media transient flow model of the circle homogeneous reservoir. They used the perturbation method to give the zero order, first order and second order perturbation solution, and gave a brief analysis of the flow characteristics in the deformable media. In the same year, Zhang et al.[14] applied the numerical method to give the pressure transient behavior characteristics of the infinite radial flow homogeneous system in pressure-sensitive reservoirs. In 1993, Yeung[15] developed a spherical transient flow model for the deformable homogeneous reservoir, and gave the approximate solution to the model. This transient flow model was applicable to some partial penetrating wells, but not accurate.

In 2000, Wu and Pruess[16] gave the integral solution of the transient flow model by considering the influence of pressure sensitivity on permeability, and compared their results with the numerical results. They pointed out that the injection pressure changed while the permeability changed with pressure. In 2001, Davies et al.[17] studied the permeability variation in pressure-sensitive reservoirs, and developed a mathematical model of the permeability variation. In 2002, Osorio and Alcalde[18] and others studied how to determine the influence of rock deformation on the formation characteristics by using well test method, and developed a 3D stress-strain model. Based on the stress-strain relation and fluid flow equations, they got the radial variation mechanics of the principal stress, the permeability and the bottom pressure by using the finite difference method. In 2003, Samaniego and Villalobos[19] gave a transient flow model for the pressure-sensitive naturally fractured res-

ervoir. The key issue they studied was the compressibility of fluid, cracks and pores. They used the pseudo-pressure method introduced by Raghanvan, which involved the permeability variation in the pseudo pressure item. They mainly solved the problem for the semi-logarithm analysis and verified their method by field examples.

In 2003, Gang and Dusseault[20] gave the variation mechanics and a mathematical model of porosity and permeability in the near wellbore regions for the pressure-sensitive reservoir. In theory, they studied the stress and pressure variation around a single production well and the near wellbore formation damage caused by the formation rock compaction. Their results showed that the production rate reduced with time, since the near wellbore formation rock compaction caused by stress. This research had a positive significance on transient flow mechanics in the pressure-sensitive reservoir. In 2007, Shunde et al.[21] gave the relationship between the pore elastic behavior and the formation pressure under super-pressure conditions. They found the formation pressure changed in different ways in various stress-sensitive formation.

Zhou et al.[22] Ge[23], Tong et al.[24], Su et al.[25], Dong[26], and Wang et al.[27] gave some theoretical analysis on various aspects of deformable reservoirs.

In recent years, with the deep exploitation of super-pressure gas reservoir in western China, the research of deformable reservoir becomes a new hot point in the oil and gas industry again. The previous research was mainly focused on the elastic and elastoplastic deformable reservoirs, and was mainly based on the theory that the permeability changes with the pressure. The research on plastic deformable reservoir was rare. Based on the previous research, this paper presents the exponential relation to describe the change of rock porosity and permeability with pressure, and establishes a transient flow model involving the porosity and permeability changes. In this paper, the finite element method is used to study the transient flow mechanics under various conditions such as various porosity, various permeability and both various porosity and permeability. The effect of changing porosity and permeability on the wellbore pressure is also analyzed. The transient flow model is verified by some field cases with approving reservoir permeability modules.

1 Mathematical model

1.1 Description of the physical model

1) The reservoir is assumed to be homogeneous and thickness-fixed, and the production is scheduled for a fixed flow rate q.

2) The fluid is single-phase and slight-compressible Newtonian fluid.

3) The fluid flow is a kind of radial flow and obeys Darcy's law, and the effects of gravity and capillary force are neglected.

4) The dual-porosity formation contains two kinds of pore. The fractures are considered as the flow channels, the fluid in the matrix is the main flow source, and the fluid flow between the matrix and fracture is steady cross flow.

5) The various permeability and porosity with the effective stress are expressed in exponential forms, both permeability modulus α_k and porosity modulus α_ϕ are assumed to be constant separately.

6) The effects of wellbore storage and skin factor in the inner boundary conditions are considered by using the effective wellbore radius model.

7) The outer boundaries may be infinite, circle and linear combination form in shape, and pressure-fixed and closed in boundary properties.

8) The whole transient flow process is isothermal.

1.2 Development of the mathematical model

1.2.1 Mass continuity equation. According to the transient flow model for the dual porosity reservoir with quasi-stable cross flow presented by Warren and Root[28], the mass continuity equation in the fracture of the pressure-sensitive fractured reservoir is

$$\frac{\partial(\rho\phi_{\mathrm{f}})}{\partial t}+\nabla\cdot(\rho V_{\mathrm{f}})-q_{\mathrm{m}}=0. \tag{1}$$

The continuity equation in the matrix is

$$\frac{\partial(\rho\phi_{\mathrm{m}})}{\partial t}+q_{\mathrm{m}}=0. \tag{2}$$

The equation of the cross flow from the matrix to the fracture is

$$q_{\mathrm{m}}=\alpha_\lambda\frac{\rho_0}{\mu}(p_{\mathrm{m}}-p_{\mathrm{f}}), \tag{3}$$

where q_{m} is the cross flow rate and α_λ is the cross flow coefficient.

1.2.2 Equation of the changing density fluid. Under isothermal condition, the fluid compressibility is defined

as

$$c_{\mathrm{f}} = -\frac{1}{V}\frac{\mathrm{d}V}{\mathrm{d}p} = \frac{1}{\rho}\frac{\mathrm{d}\rho}{\mathrm{d}p}.$$

By integrating the definition formula of the fluid compressibility, the state equation is

$$\rho = \rho_0 \mathrm{e}^{-c_{\mathrm{f}}(p_{\mathrm{i}}-p)}. \tag{4}$$

When the pressure variation is small, the state equation can be simplified as

$$\rho = \rho_0[1 + c_{\mathrm{f}}(p_{\mathrm{i}} - p)].$$

1.2.3 Equations of the changing porosity. In 1953, Hall defined the rock effective compressibility by experiment data, that is, the relative pore volume change with the unit pressure:

$$c_p = \frac{1}{V_p}\frac{\mathrm{d}V_p}{\mathrm{d}p}.$$

An equivalent expression of the above formula is

$$C_\phi = \frac{1}{\phi}\frac{\mathrm{d}\phi}{\mathrm{d}p}.$$

By integrating the definition formula of the pore compressibility, the state equation is

$$\phi = \phi_0 \mathrm{e}^{-C_\phi(p_{\mathrm{i}}-p)}. \tag{5}$$

When the pressure variation is small, the state equation can be simplified as

$$\phi = \phi_0[1 + C_\phi(p_{\mathrm{i}} - p)].$$

For fractured media and porous media, the porosity change can respectively be presented as

$$\begin{aligned} \phi_f &= \phi_{f0}\mathrm{e}^{-C_{\phi\mathrm{f}}(p_{\mathrm{i}}-p)}, \\ \phi_{\mathrm{m}} &= \phi_{\mathrm{m}0}e^{-C_{\phi\mathrm{m}}(p_{\mathrm{i}}-p)}. \end{aligned} \tag{6}$$

1.2.4 Equation of the changing permeability. Experimental results show that under high temperature and high pressure conditions, the relation between the rock permeability and pressure can be expressed by

$$\alpha_k = \frac{1}{k_0}\frac{\mathrm{d}k}{\mathrm{d}p}, \tag{7}$$

where α_k is named rock deformation coefficient or permeability modulus.

By integrating the formula of deformation coefficient, the state equation is

$$k = k_0 \mathrm{e}^{-\alpha_k(p_{\mathrm{i}}-p)}. \tag{8}$$

For the fractured media, the change of permeability is

$$k_{\mathrm{f}} = k_{\mathrm{f}0}\mathrm{e}^{-\alpha_{\mathrm{f}}(p_{\mathrm{i}}-p)}. \tag{9}$$

Because the permeability of the matrix is far less than that of fracture, matrix permeability is neglected in our model just like the steady model developed by Warren & Root.

1.2.5 Equation of the fluid flow rate. The fluid flow rate in fracture can be expressed by Darcy law:

$$V_{\mathrm{f}} = -\frac{k_{\mathrm{f}}}{\mu}\nabla p_{\mathrm{f}}. \tag{10}$$

1.3 The dimensional mathematical model

By substituting the fluid flow rate equation and state equation into the mass continuity equations eqs. (1)—(3), the fluid flow control equation can be expressed as follows.

The transient flow equation is

$$\phi_{\mathrm{f}0}\rho_0\frac{\partial\left(\mathrm{e}^{(C_{\phi\mathrm{f}}+C_{\mathrm{f}})(p-p_{\mathrm{i}})}\right)}{\partial t} - \frac{k_0\rho_0}{\mu}\frac{\partial}{\partial x_i}\left[\mathrm{e}^{(\alpha_{\mathrm{f}}+C_{\mathrm{f}})(p-p_{\mathrm{i}})}\frac{\partial p_{\mathrm{f}}}{\partial x_i}\right]$$
$$-\frac{\alpha_\lambda\rho_0}{\mu}(p_{\mathrm{m}} - p_{\mathrm{f}}) = 0. \tag{11}$$

The cross flow equation is

$$\phi_{\mathrm{m}0}\rho_0\frac{\partial\left(\mathrm{e}^{(\alpha_{\phi\mathrm{m}}+\alpha_\rho)(p-p_{\mathrm{i}})}\right)}{\partial t} + \frac{\alpha_\lambda\rho_0}{\mu}(p_{\mathrm{m}} - p_{\mathrm{f}}) = 0. \tag{12}$$

The initial condition is

$$p_{\mathrm{f}} = p_{\mathrm{m}} = p_{\mathrm{i}}, \ \text{at} \ t = 0. \tag{13}$$

The inner boundary conditions are

$$qB = \left[C\frac{\mathrm{d}p_{\mathrm{w}}}{\mathrm{d}t} - \frac{2\pi h}{\mu}k(p_{\mathrm{f}})\left(r\frac{\partial p_{\mathrm{f}}}{\partial r}\right)\right], \ \text{at} \ r = r_{\mathrm{w}}, \tag{14}$$

$$p_{\mathrm{w}} = \left[p_{\mathrm{f}} - Sr\frac{\mathrm{d}p_{\mathrm{w}}}{\mathrm{d}r}\right], \ \text{at} \ r = r_{\mathrm{w}}. \tag{15}$$

The outer boundary conditions are

$$p_{\mathrm{f}} = p_{\mathrm{m}} = p_{\mathrm{i}},$$
$$\text{while} \ r \to \infty \ \text{(for infinite reservoir)}, \tag{16}$$

$$p_{\mathrm{f}} = p_{\mathrm{m}} = p_{\mathrm{i}},$$
$$\text{at} \ r = r_{\mathrm{e}} \ \text{(for pressure-fixed circle boundary)}, \tag{17}$$

$$\frac{\partial p_{\mathrm{f}}}{\partial r} = \frac{\partial p_{\mathrm{m}}}{\partial r} = 0,$$
$$\text{at} \ r = r_{\mathrm{e}} \ \text{(for closed circle boundary)}, \tag{18}$$

$$p_{\mathrm{f}} = p_{\mathrm{m}} = p_{\mathrm{i}}, \ \text{while} \ x, y \in \Gamma_i$$
$$\text{(for pressure-fixed linear boundary)}, \tag{19}$$

$$\frac{\partial p_{\mathrm{f}}}{\partial n} = \frac{\partial p_{\mathrm{m}}}{\partial n} = 0, \ \text{while} \ x, y \in \Gamma_j$$
$$\text{(for closed linear boundary)}, \tag{20}$$

where B is the fluid volume factor, $\mathrm{m}^3/\mathrm{m}^3$. C is the

wellbore storage coefficient, m^3/MPa. C_t is the total compressibility, m^3/MPa. h is the net pay of the formation, m. k is the reservoir permeability, μm^2. p is the reservoir pressure, MPa. p_f is the pressure in the fracture, MPa. p_i is the initial pressure of the reservoir, MPa. p_m is the pressure in the matrix, MPa. p_w is the wellbore pressure, MPa. q is the production rate of the well, m^3/d. r is the distance, m. S is the skin factor, 1. ϕ_m is the porosity of the matrix, 1. μ is the viscosity of the fluid, mPa·s. ρ_0 is the reference density of the fluid, kg/m^3. Γ_i as well as Γ_j is the liner boundary.

1.4 The dimensionless mathematical model

1.4.1 The dimensionless process of the mathematical model. In order to obtain a more universal transient flow model, we change the mathematical model into dimensionless form. The dimensionless mathematical model is expressed as follows.

The dimensionless fluid flow control equation is

$$\omega e^{-C_{tfD}p_{fD}}\frac{\partial p_{fD}}{\partial t_D}-\frac{\partial}{\partial x_{iD}}\left[e^{-\alpha_{tkD}p_{fD}}\frac{\partial p_{fD}}{\partial x_{iD}}\right]-\lambda(p_{mD}-p_{fD})=0. \tag{21}$$

The cross flow equation is

$$(1-\omega)e^{-C_{tmD}p_{mD}}\frac{\partial p_{mD}}{\partial t_D}+\lambda(p_{mD}-p_{fD})=0. \tag{22}$$

The initial condition is

$$p_{fD}=p_{mD}=0,\quad \text{at}\quad t_D=0. \tag{23}$$

The inner boundary conditions are

$$-1=C_D\frac{\partial p_{wD}}{\partial t_D}+e^{-\alpha_{tfD}p_{fD}}\frac{\partial p_{fD}}{\partial r_D},\quad \text{at}\quad r_D=1, \tag{24}$$

$$p_{wD}=\left[p_{fD}-Sr_D\frac{dp_{wD}}{dr_D}\right],\quad \text{at}\quad r_D=1. \tag{25}$$

The outer boundary conditions are

$$p_{fD}=p_{mD}=0,\quad \text{while}\quad r_D\to\infty$$
(for infinite reservoir), (26)

$$p_{fD}=p_{mD}=0,\quad \text{at}\quad r_D=r_{eD}$$
(for pressure-fixed circle boundary), (27)

$$\frac{\partial p_{fD}}{\partial r_D}=\frac{\partial p_{mD}}{\partial r_D}=0,\quad \text{at}\quad r_D=r_{eD}$$
(for closed circle boundary), (28)

$$p_{fD}=p_{mD}=0,\quad \text{while}\quad x_D,y_D\in\Gamma_i$$
(for pressure-fixed linear boundary), (29)

$$\frac{\partial p_{fD}}{\partial n}=\frac{\partial p_{mD}}{\partial n}=0,\quad \text{while}\quad x_D,y_D\in\Gamma_i$$
(for closed linear boundary), (30)

where the dimensionless parameters are defined as

Dimensionless pressure in the fracture:

$$p_{fD}=\frac{hk_{f0}}{1.842\times10^{-3}qB\mu}(p_i-p_f).$$

Dimensionless pressure in the matrix:

$$p_{mD}=\frac{hk_{f0}}{1.842\times10^{-3}qB\mu}(p_i-p_m).$$

Dimensionless distance:

$$r_D=\frac{r}{r_w},\quad x_D=\frac{x}{r_w},\quad y_D=\frac{y}{r_w}.$$

Dimensionless time: $t_D=\dfrac{3.6k_{f0}}{(\phi_fC_{tf}+\phi_mC_{tm})\mu r_w^2}t.$

Dimensionless wellbore storage coefficient:

$$C_D=\frac{C}{2\pi h(\phi_fC_{tf}+\phi_mC_{tm})r_w^2}.$$

Dimensionless reserve storage ratio:

$$\omega=\frac{\phi_fC_{tf}}{\phi_fC_{tf}+\phi_mC_{tm}}.$$

Dimensionless cross flow coefficient: $\lambda=\dfrac{\alpha_\lambda}{k_{f0}}r_w^2.$

Dimensionless deformation coefficient:

$$\beta=\frac{1.842\times10^{-3}\alpha_k qB\mu}{k_0h}.$$

1.4.2 Quasi-linearization of the mathematical model. As a matter of convenience to solve the mathematical model, the method of quasi-linearization is used to handle the nonlinear equations. The results obtained are expressed as follows:

$$\frac{\omega}{C_De^{2S}}\frac{\partial U_f}{\partial T_D}-\frac{\partial}{\partial x_{iD}}\left[U_f^{\frac{\alpha_{tkD}}{C_{tf}}-1}\frac{\partial U_f}{\partial x_{iD}}\right]-\lambda_D\left(\frac{C_{tf}}{C_{tm}}U_m-U_f\right)=0. \tag{31}$$

$$\frac{1-\omega}{C_De^{2S}}\frac{C_{tf}}{C_{tm}}\frac{\partial U_m}{\partial t_D}+\lambda\left(\frac{C_{tf}}{C_{tm}}U_m-U_f\right)=0. \tag{32}$$

The initial condition:

$$U_f(R_D,0)=U_m(R_D,0)=1. \tag{33}$$

The inner boundary conditions is

$$R_D\frac{\partial U_f}{\partial R_D}\Big|_{R_D=1}=\beta+\frac{1}{U_f}\frac{\partial U_f}{\partial T_D}. \tag{34}$$

The outer boundary conditions are

$$U_{\mathrm{f}}\left(R_{\mathrm{D}}\to\infty,T_{\mathrm{D}}\right)=U_{\mathrm{m}}\left(R_{\mathrm{D}}\to\infty,T_{\mathrm{D}}\right)=1$$

(for infinite reservoir), (35)

$$U_{\mathrm{f}}\left(R_{e\mathrm{D}},T_{\mathrm{D}}\right)=U_{\mathrm{m}}\left(R_{e\mathrm{D}},T_{\mathrm{D}}\right)=1$$

(for pressure-fixed circle boundary), (36)

$$\frac{\partial U_{\mathrm{f}}\left(R_{e\mathrm{D}},T_{\mathrm{D}}\right)}{\partial R_{\mathrm{D}}}=\frac{\partial U_{\mathrm{m}}\left(R_{e\mathrm{D}},T_{\mathrm{D}}\right)}{\partial R_{\mathrm{D}}}=0$$

(for closed circle boundary), (37)

$$U_{\mathrm{fD}}=U_{\mathrm{mD}}=1,\ \text{while}\ \ x_{\mathrm{D}},y_{\mathrm{D}}\in\Gamma_i$$

(for pressure-fixed linear boundary), (38)

$$\frac{\partial U_{\mathrm{fD}}}{\partial n}=\frac{\partial U_{\mathrm{mD}}}{\partial n}=0,\ \text{while}\ \ x_{\mathrm{D}},y_{\mathrm{D}}\in\Gamma_i$$

(for closed linear boundary), (39)

where $T_{\mathrm{D}}=t_{\mathrm{D}}/C_{\mathrm{D}}$, $U_{\mathrm{f}}=\mathrm{e}^{-C_{t\mathrm{fD}}p_{\mathrm{fD}}}$, $U_{\mathrm{m}}=\mathrm{e}^{-C_{t\mathrm{mD}}p_{\mathrm{mD}}}$, $R_{\mathrm{D}}=\dfrac{r}{r_{\mathrm{w}}\mathrm{e}^{-S}}$, $\lambda_{\mathrm{D}}=\lambda\mathrm{e}^{-2S}$.

2 Solution of the mathematical model

2.1 Finite element method

To solve the above mathematical model, Galerkin finite element method with weighted residual and selected interpolation function φ_i as weight function is used. The dimensionless model is changed into the finite element equations:

$$\iint_A\varphi_i^{\mathrm{e}}\left\{\frac{\omega}{C_{\mathrm{D}}\mathrm{e}^{2S}}\frac{\partial U_{\mathrm{f}}^{\mathrm{e}}}{\partial T_{\mathrm{D}}}-\frac{\partial}{\partial x_{i\mathrm{D}}}\left[U_{\mathrm{f}}^{e\,\frac{\alpha_{tk\mathrm{D}}}{C_{t\mathrm{f}}}-1}\frac{\partial U_{\mathrm{f}}^{\mathrm{e}}}{\partial x_{i\mathrm{D}}}\right]\right.$$

$$\left.-\lambda_{\mathrm{D}}\left(\frac{C_{t\mathrm{f}}}{C_{t\mathrm{m}}}U_{\mathrm{m}}^{\mathrm{e}}-U_{\mathrm{f}}^{\mathrm{e}}\right)\right\}\mathrm{d}A=0\ \ (i=1,2,3), \tag{40}$$

$$\iint_A\varphi_{\mathrm{i}}^{\mathrm{e}}\left[\frac{1-\omega}{C_{\mathrm{D}}\mathrm{e}^{2S}}\frac{C_{t\mathrm{f}}}{C_{t\mathrm{m}}}\frac{\partial U_{\mathrm{m}}^{\mathrm{e}}}{\partial t_{\mathrm{D}}}+\lambda\left(\frac{C_{t\mathrm{f}}}{C_{t\mathrm{m}}}U_{\mathrm{m}}^{\mathrm{e}}-U_{\mathrm{f}}^{\mathrm{e}}\right)\right]\mathrm{d}A=0$$

$$(i=1,2,3), \tag{41}$$

where φ_i^{e} is element linear interpolation function and

$$\varphi_{\mathrm{i}}^{\mathrm{e}}=a_i+b_ix+c_iy,\quad i=1,\ 2,\ 3.$$

$$\frac{\partial\varphi_1^{\mathrm{e}}}{\partial x}=b_1,\quad\frac{\partial\varphi_2^{\mathrm{e}}}{\partial x}=b_2,\quad\frac{\partial\varphi_3^{\mathrm{e}}}{\partial x}=b_3;$$

$$\frac{\partial\varphi_1^{\mathrm{e}}}{\partial y}=c_1,\quad\frac{\partial\varphi_2^{\mathrm{e}}}{\partial y}=c_2,\quad\frac{\partial\varphi_3^{\mathrm{e}}}{\partial y}=c_3;$$

$$a_1=\frac{1}{2A}(x_2y_3-x_3y_2),\quad a_2=\frac{1}{2A}(x_3y_1-x_1y_3),$$

$$a_3=\frac{1}{2A}(x_1y_2-x_2y_1);$$

$$b_1=\frac{1}{2A}(y_2-y_3),\ b_2=\frac{1}{2A}(y_3-y_1),$$

$$b_3=\frac{1}{2A}(y_1-y_2);$$

$$c_1=\frac{1}{2A}(x_3-x_2),\quad c_2=\frac{1}{2A}(x_1-x_3),$$

$$c_3=\frac{1}{2A}(x_2-x_1).$$

A is the triangle area:

$$A=\frac{1}{2}\begin{vmatrix}1&1&1\\x_1&x_2&x_3\\y_1&y_2&y_3\end{vmatrix}$$

$$=\frac{1}{2}\left(x_2y_3+x_1y_2+x_3y_1-x_2y_1-x_3y_2-x_1y_3\right),$$

$$U^{\mathrm{e}}=U_1^{\mathrm{e}}\varphi_1^{\mathrm{e}}+U_2^{\mathrm{e}}\varphi_2^{\mathrm{e}}+U_3^{\mathrm{e}}\varphi_3^{\mathrm{e}},$$

where U_1^{e}, U_2^{e} and U_3^{e} are the values at the three element nodes respectively. From the above equation, we can easily derive the following equations:

$$\frac{\partial U^{\mathrm{e}}}{\partial x}=U_1^{\mathrm{e}}\frac{\partial\varphi_1^{\mathrm{e}}}{\partial x}+U_2^{\mathrm{e}}\frac{\partial\varphi_2^{\mathrm{e}}}{\partial x}+U_3^{\mathrm{e}}\frac{\partial\varphi_3^{\mathrm{e}}}{\partial x}; \tag{42}$$

$$\frac{\partial U^{\mathrm{e}}}{\partial y}=U_1^{\mathrm{e}}\frac{\partial\varphi_1^{\mathrm{e}}}{\partial y}+U_2^{\mathrm{e}}\frac{\partial\varphi_2^{\mathrm{e}}}{\partial y}+U_3^{\mathrm{e}}\frac{\partial\varphi_3^{\mathrm{e}}}{\partial y}. \tag{43}$$

Finally, we get the system equations from assembling the element equations. By solving the system equation, the value $U(x,y)$ at the node (x,y) at time step n+1 can be calculated. So the pressure value $p(x,y)$ can be easily calculated from $U(x,y)$.

2.2 Mesh generation

In order to get the appropriate solution of the definite problem, the finite element method is used to solve the differential equations. The solution area needs to be discretized in terms of nodes, lines or planes first. In this paper, the unstructured triangular grid self-adaptive technology presented in 1990s is used to discretize the research region. The technology is the improved method of Delaunay triangulation based on Watson algorithm. For the transient seepage problem near a single well, the pressure gradient near-wellbore is much larger than that at the point far from the well. Therefore, mesh densification in the near-wellbore region is needed to ensure the accuracy of the solution while relatively coarse grids can be used in distant area. Figure 1 gives the triangular grids of single well with circle outer boundary for radial flow. Figure 2 represents the amplified grids in the near-

wellbore region. The mesh near-wellbore can be thickened in an arbitrary way.

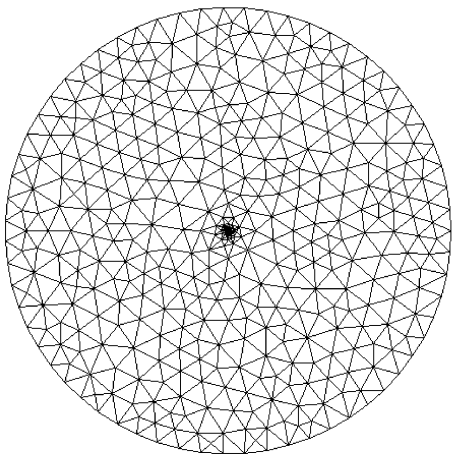

Figure 1 The triangular grids for the circle reservoir.

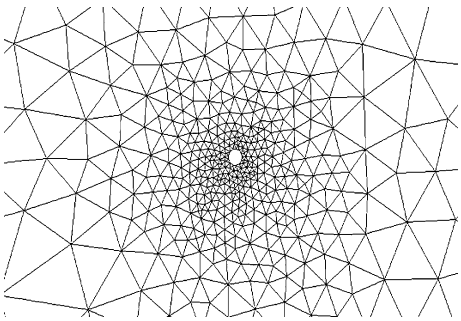

Figure 2 The grids in the near-wellbore region.

2.3 Finite element program design

The computer program frame for solving the mathematical model of well test analysis by using the finite element method is shown in Figure 3. According to the computer diagram in Figure 3, the corresponding finite element calculation program is compiled. The double logarithm curves that reflect the change of the wellbore pressure and pressure derivative with time are calculated by using the finite element method.

3 Characteristics analysis of type curves

3.1 Type curves for the infinite pressure-sensitive fractured reservoir

Based on the transient flow model for the pressure-sensitive fractured reservoir, we get the type curves of the wellbore pressure with four conditions: (1) just considering permeability variation; (2) just considering the porosity variation; (3) considering both permeability and porosity variation; (4) considering neither permeability nor porosity variation. These four kinds of type curves are shown as Figure 4.

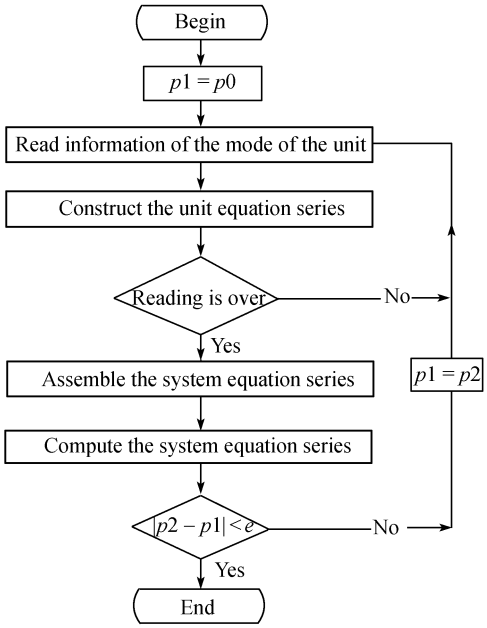

Figure 3 The finite element program diagram.

Figure 4 shows that: (1) Only with porosity variation, the type curves of the wellbore pressure and its derivative in the pressure-sensitive reservoir is similar to that of non-pressure-sensitive reservoir. This is in agreement with the experimental results. In other words, this comparison presented here obviously verifies the correctness of our model in this paper. (2) The type curve with mere permeability change is similar to the one with the simultaneous change of permeability and porosity, which is in accordance with the experiments. This conclusion can be explained that the porosity has little influence on the type curve. (3) If the pressure-sensitive effect is considered only, there will be certain difference between the type curves for the pressure-sensitive reservoir and that of the non-pressure-sensitive reservoir. These conclusions coincide with the present qualitative understanding and the results are quantitatively expressed in this paper.

3.2 Type curves for the closed circle pressure-sensitive fractured reservoir

Based on the transient flow model for the pressure-sensitive fractured reservoir, the type curves with permeability modulus change in the closed circle boundary condition are got, shown as Figure 5, from which, we

can see that: (1) With the increase of the permeability modulus, the pressure curve of the pressure-sensitive reservoir deviates upwards from that of non-pressure-sensitive reservoir, while the pressure derivative curve of the pressure-sensitive reservoir deviates downwards from that of non-pressure-sensitive reservoir. (2) With the increase of the pressure-sensitive fractured reservoir permeability modulus, the distance between the pressure curve and the pressure derivative curve increase. Thus, it can be inferred that the skin factor will be not correctly explained by conventional well test interpretation software. (3) With the increase of the permeability modulus, the effect on the boundary reflect time is not obvious.

In addition, from the pressure derivative curve in Figure 5, we can see that the type curves can be divided into 5 sections:

(1) Pure wellbore storage section: Both the slopes of the pressure and the pressure derivative curve are equal to 1.0.

(2) The after flow and pressure-sensitive effect interaction section: With the permeability modulus increase, the time of transition section gradually reduces.

(3) Dual-porosity characteristics reflection section: There is an almost symmetrical hollow region in the pressure derivative curve, which is the same as the conventional dual-porosity reservoir.

(4) The infinite radial flow section: The pressure derivative curve is very different from that of conventional infinite homogeneous reservoir. The pressure derivative of conventional infinite homogeneous reservoir is equal to constant 0.5, but that of the pressure-sensitive reser-

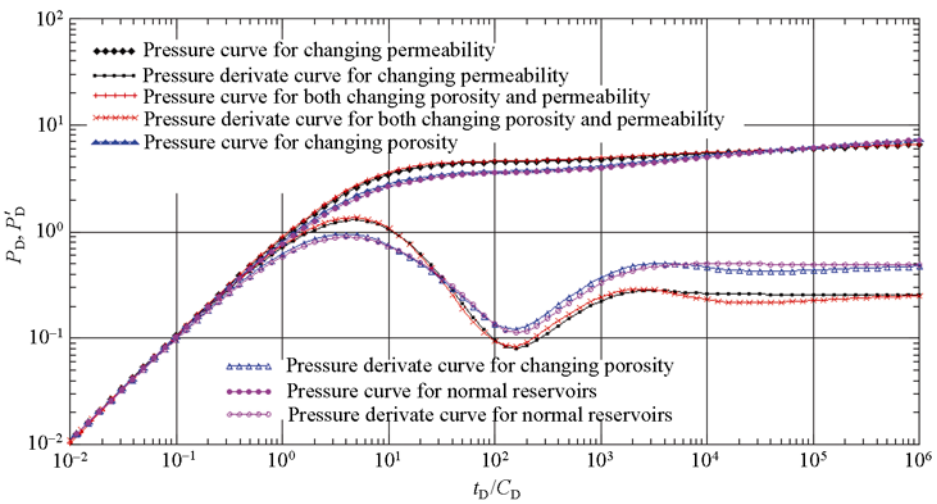

Figure 4 The type curves of the infinite pressure-sensitive fractured reservoir.

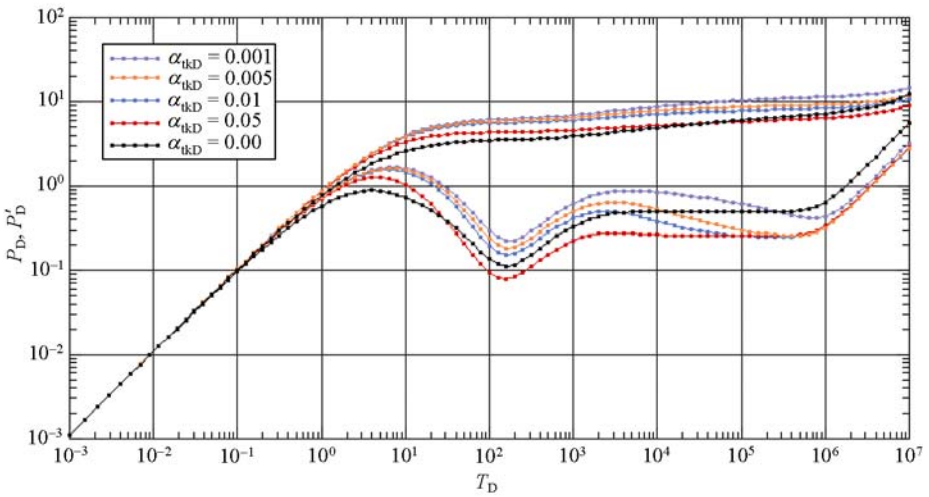

Figure 5 The type curves of pressure and pressure derivative for the closed circle pressure-sensitive reservoir (CDE2S = 1, ω = 0.01, λ = 0.01).

voir is equal to a constant which is smaller than 0.5.

(5) Outer boundary reflecting section: For closed circle reservoir, the pressure derivative curve upwarps when the pressure wave reaches the outer boundary, and the pressure curve and its derivative curve merge into a straight line with the slope of 1.0.

3.3 Type curves for the pressure-sensitive fractured reservoir with linear combination quadrilateral boundaries

In order to verify the correctness of mathematical model and the practicality of calculation method, the type curves of the pressure-sensitive fractured reservoir with linear combination quadrilateral outer boundaries are calculated in this paper. In the calculating region, there are three closed linear boundaries and one pressure-fixed boundary. Figure 6 shows the grids of the domain and Figure 7 describes the type curves. Figure 7 shows that when the pressure wave reaches the closed boundaries, the pressure declines, but the pressure difference increases and both pressure curve and pressure derivative curve go upwarps. And when the pressure wave reaches pressure-fixed boundary, the pressure keeps steady, but the pressure derivative decline. This conclusion is in accordance with the boundary reflection of the non-pressure-sensitive reservoir.

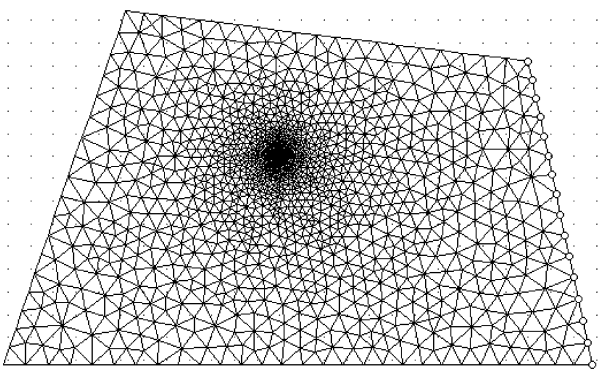

Figure 6 The grids in the solution region.

3.4 Simplified analysis of the type curves for the pressure-sensitive fractured reservoir

The transient flow model for the pressure-sensitive fractured reservoir in this paper can be simplified as that of pressure-sensitive homogenous sandstone reservoir. Therefore, the obtained results are somewhat universal. The degenerate type curves of pressure and pressure derivative are given in Figure 8.

4 The field case of well test data analysis for the pressure-sensitive fractured reservoir

In order to verify the correctness of mathematical model and the practicality of numerical method for the pressure-sensitive fractured reservoir, some field test data in the high pressure deep wells are analyzed and good analysis results are got. These results have been used in the oilfield development plan's design. Here, we show the application of the transient flow model for pressure-sensitive fractured reservoir by one of the field cases.

4.1 Introduction of one well in some oil field

The well completed in the formation at depth of 5101 m, and belongs to the high-pressure ultra-deep well and is very difficult to test. It took 12 days to accomplish the well test to get the test data. The whole test history data is shown in Figure 9.

4.2 Well test analysis results

According to the well test analysis requirement, it is necessary to get correct analysis results for matching the double logarithm, semi-logarithm superposition and whole history all perfectly. Our analysis fitting graphs are presented in Figures 10—12.

4.3 Evaluation of the well test results

The comparison between our analysis results and conventional analysis results are shown in Table 1. Seen from the table, except the permeability has lager difference, the skin factor has the largest difference, which is in accordance with the result from above theoretical analysis. According to the field analysis, the skin factor of 63.46 expresses the formation damaged seriously. But the formation in this region actually has not been damaged, it is only a kind of fractured reservoir with some pressure-sensitive characteristics as the production formation is 5000 m under ground. This conclusion is proved very well by the indoor core experiments.

In addition, an important parameter, namely permeability modulus, is obtained in this paper. It can be directly applied to the well productivity rate prediction. The field application results show that the production rate predicted by using the permeability modulus in our study perfectly agrees with the actual production situation.

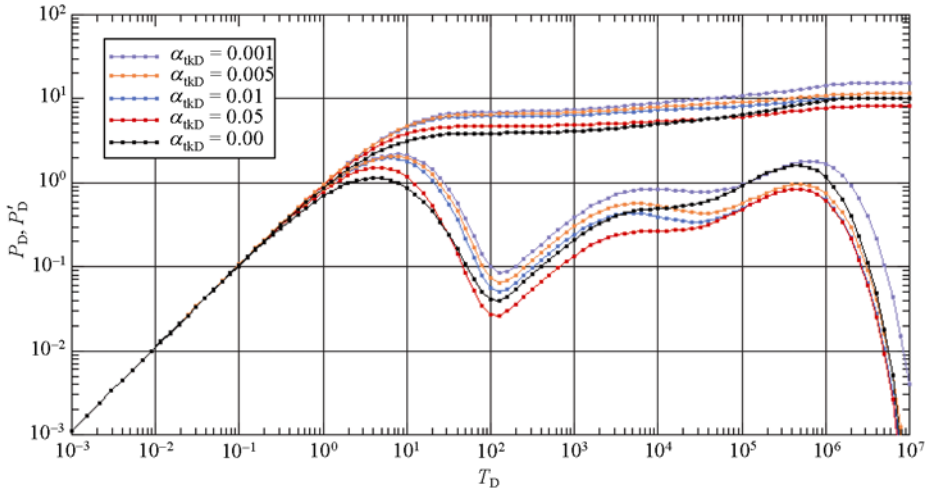

Figure 7 The type curves of combination quadrilateral boundaries (CDE2S = 1, ω = 0.05, λ = 0.05).

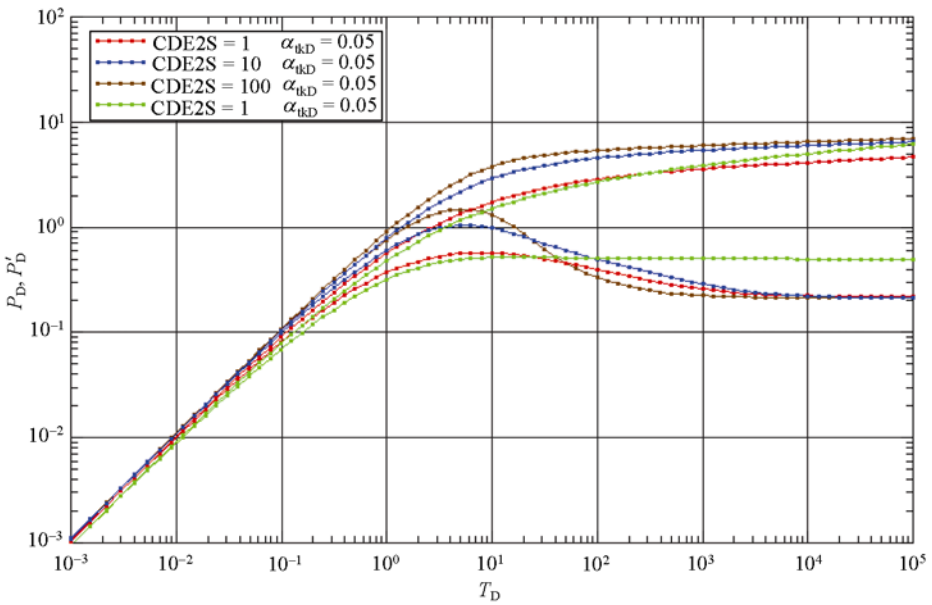

Figure 8 The type curves for the pressure-sensitive homogenous sandstone reservoir (α = 0.00, CDE2S = 1).

Table 1 The comparative analysis of the well test results

Parameter name	Our analysis results	Conventional analysis results
Flow coefficient (um^2·m/mPa·s)	0.7925	2.0972
Reservoir factor (um^2·m)	0.03065	
Reservoir permeability (um^2)	14.95×10^{-3}	39.21×10^{-3}
Reserve storage coefficient	0.06	/
Cross flow coefficient	0.3×10^{-3}	/
Permeability modulus (MPa^{-1})	0.01921	/
Wellbore storage coefficient (m^3/MPa)	8.291×10^{-3}	1.597×10^{-6}
Skin factor	–1.485	63.46
Reservoir pressure (MPa)	105.2	105.063

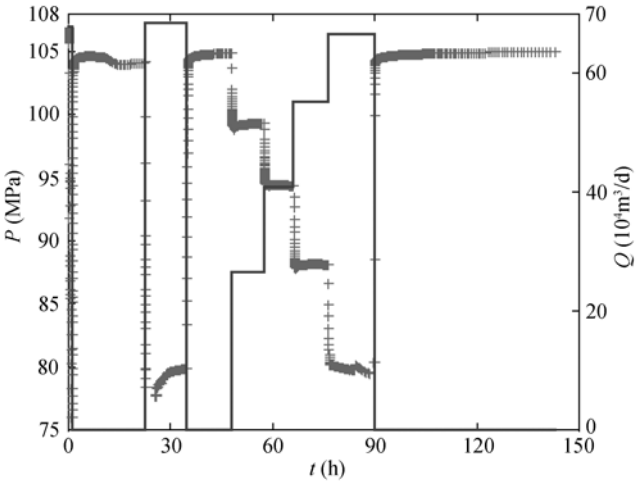

Figure 9 The well test pressure and flow rate history.

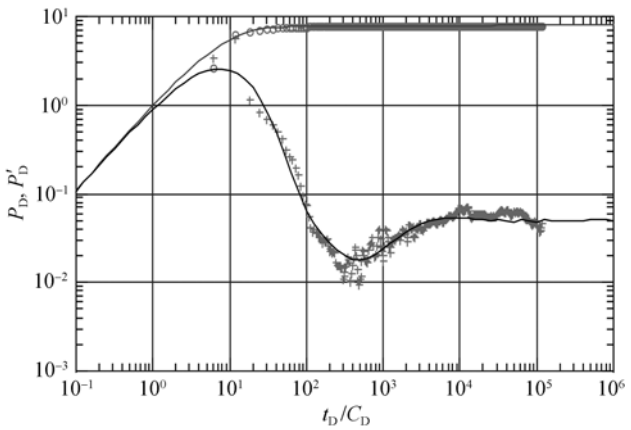

Figure 10 The double logarithm matching diagram.

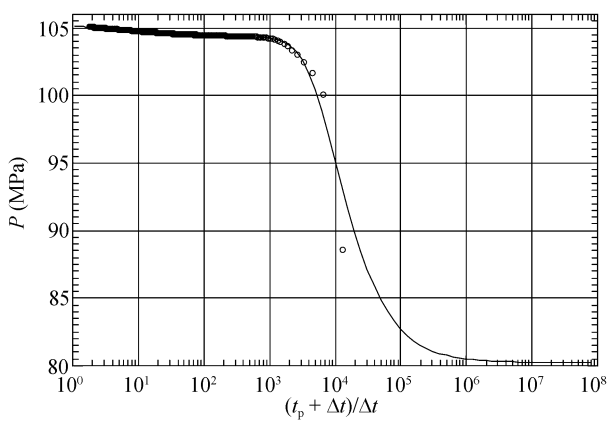

Figure 11 The semi-logarithm superposition verification diagram.

5 Conclusions

The transient flow model presented in this paper has been successfully applied to the real reservoirs. Numerical method is capable of producing highly accurate and reliable solutions. The conclusions can be drawn below:

(1) According to the current experimental results and the pressure-sensitive fractured reservoir properties, the transient flow model with various outer boundary conditions for the pressure-sensitive fractured reservoir is established.

(2) The finite element equation of the transient flow model for the pressure-sensitive fractured reservoir is derived.

(3) Based on the unstructured grids of the research regions applied, we calculate the wellbore pressure curves for the pressure-sensitive fractured reservoir with different outer boundaries, such as infinite boundary, circle boundary and combined linear boundaries are calculated by using the finite element method. The characteristics of the type curves are comparatively analyzed.

(4) The effects on the pressure curves cased by pressure sensitivity coefficient and the effective wellbore radius combined parameter $C_D e^{2S}$ are determined. The method for calculating the reservoir factor of the pressure-sensitive reservoir is introduced.

(5) By analyzing the well test data of a gas well in the high temperature and high pressure deep reservoir, we get good analysis results. The correctness of the transient flow model for the pressure-sensitive fractured reservoir in this paper is verified.

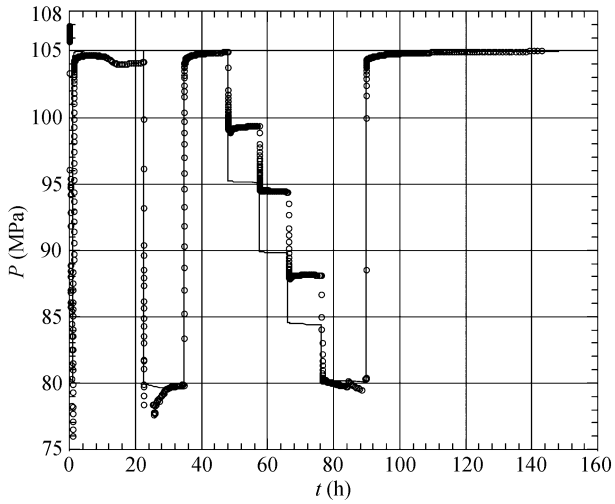

Figure 12 The whole history matching diagram.

1 Thomas R D, Wardd D C. Effect of overburden pressure and water saturation on gas permeability of tight sandstone cores. J Pet Technol, 1972, 24(2): 120－124

2 Jones F O, Owens W W. A laboratory study of the low permeability

gas sands. J Pet Technol, 1980, 32(9): 1631－1640
3 Kilmer N H, Morrow N R, Pitman J K. Pressure sensitivity of low permeability sandstones. J Pet Sci Eng, 1987, 1(1): 65－81[DOI]
4 Vairogs J, Hearn C L, Dareing D W, et al. Effect of rock stress on gas production from low-permeability reservoirs. J Pet Technol, 1971, 23(9): 1161－1167
5 Terzaghi K. Theoretical Soil Mechanics. New York: Wiley, 1943
6 Biot M A. General theory of three-dimensional consolidation. J Appl Phys, 1941, 12(2): 155－164[DOI]
7 Geertsma J. The effect of fluid pressure decline on volumetric changes of porous rocks. Trans AIME, 1957, 210(3): 403－524
8 Finol A, Farouq Ali S M. Numerical simulation of oil production with simultaneous ground subsidence. Soc Pet Eng J, 1975, 15(10): 411－424
9 Горбунов A T. The Development of Abnormal Reservoir (in Chinese). Zhang S B, trans. Beijing: Petroleum Industry Press, 1981. 18－42
10 Raghavan R, Scorer D T, Miller F G. An investigation by numerical methods of the effect of pressure-dependent rock and fluid properties. Soc Pet Eng J, 1972, 12(6): 167－176
11 Samaniego V F, Brigham W E, Miller F G. An investigation of transient flow of reservoir fluids considering pressure-dependent rock and fluid properties. Soc Pet Eng J, 1977, 17(4): 140－149
12 Ostensen R W. Micro-crack permeability in tight gas sand-stone. Soc Pet Eng J, 1983, 23(12): 66－69
13 Pedrosa O A Jr. Pressure transient response in stress-sensitive formations. SPE 15115. The 1986 California Regional Meeting, Oakland, CA, 2-4, April, 1986
14 Zhang M Y, Ambastha A K. New insights in pressure transient analysis for stress sensitive reservoir. SPE 28420. The 69th Annual Technical Conference and Exhibition held in New Orleans, LA, USA, 25-28, Sept. 1994. 617－627
15 Yeung K. An approximate analytical study of aquifers with pressure-sensitive formation permeability. Water Resour Res, 1993, 29(10): 3495－3501[DOI]
16 Wu Y S, Pruess K. Integral solutions for transient fluid flow through a porous medium with pressure-dependent permeability. Int J Rock Mech Min Sci, 2000, 37(1-2): 51－61[DOI]
17 Davies J P, Davies D K. Stress-dependent permeability: Characterization and modeling. SPE 71750. Soc Pet Eng J, 2001, 36(6): 224－235
18 Osorio J G, Alcalde O R. A numerical model to study the formation damage by rock deformation from well test analysis. SPE 73742. The SPE International Symposium and Exhibition on Formation Damage Control, Lafayette, Louisiana, USA, 20－21 Feb, 2002
19 Samaniego V F, Villalobos L H. Transient pressure analysis of pressure-dependent naturally fractured reservoirs. J Pet Sci Eng, 2003, 39(1-2): 45－56[DOI]
20 Gang H, Dusseault M B. Description of fluid flow around a wellbore with stress-dependent porosity and permeability. J Pet Sci Eng, 2003, 40(1-2): 1－16[DOI]
21 Shunde Y, Dusseaultb M B, Rothenburg L. Analytical and numerical analysis of pressure drawdown in a poroelastic reservoir with complete overburden effect considered. Adv Water Resour, 2007, 30(5): 1160－1167 [DOI]
22 Zhou R, Liu Y W, Zhou F X. Numerical solutions for the transient flow in the homogeneous closed circle reservoirs. Acta Mech Sin, 2003, 19(1): 40－45[DOI]
23 Ge J L. The Mechanics of Fluid Flow in Reservoir (in Chinese). Beijing: Petroleum Industry Press, 1982
24 Tong D K, Jiang D M, Chen X L. Dynamic characters in dual-porosity deformation reservoir (in Chinese). J Univ Pet, 2005, 25(5): 53－56
25 Su Y L, Zhang Y G. The development character in deformation reservoir (in Chinese). Acta Petrolei Sin, 2000, 21(2): 51－55
26 Dong P C. Numerical model of fully coupled fluid solid seepage in a deformable porous media and its application (in Chinese). J Geomech, 2005, 11(3): 273－277
27 Wang Y F, Liu Y W, Jia Z Q. Well test analysis under the changing porousity and permeability caused by deformable formation (in Chinese). J Xi'an Shiyou Univ (Nature Science), 2004, 19(2): 17－20
28 Warren J E, Root P J. Behavior of naturally fractured formations. Soc Pet Eng J, 1963, 3(9): 245－255